Chemistry and Materials Research
ISSN 2224- 3224 (Print) ISSN 2225- 0956 (Online)
Vol.17 No.1, 2025

Revealing the chemical role of Al promoter with extremely low content of 0.85% in Fe_2O_3 for the High-Temperature Water-Gas Shift Reaction

Binbin Qian*, Xue Wang, Yiling Luo, Feifei Lu, Yujin Liu, Zongtang Liu, Zhenghao Fei
School of Chemistry and Environmental Engineering, Yancheng Teachers University
Yancheng 224007, China
E-mail: qianbb@yctu.edu.cn

Abstract

The high-temperature water-gas shift (HT-WGS) reaction is critically important for the development of H_2 production and Al is conventionally considered as a textural promoter to stabilize the surface of the iron oxide phase towards sintering. Here in this paper, we found that Al can also be a chemical promoter with an extremely low content of 0.85% in Fe_2O_3. The results show that due to the addition of Al (from 0.34 to 4.42%), the spinel structured $FeAl_2O_4$ formed, which can grasp Fe^{2+} and thus improved the CO conversion by redox mechanism. Lower content of Al with the amount of 0.85% ($Fe_{1.95}Al_{0.05}O_3$) exhibited the best activity in terms of CO conversion for HT-WGS at 400 ℃ and 450 ℃. Scanning transmission electron microscopy (STEM) confirmed that atomic isolation of Al atoms within Fe_3O_4 lattice not only optimizes the hydrogen-binding energy but also decreases the free energy of water formation, thus leading to excellent thermocatalytic activity of Al1-Fe_2O_3 catalyst. The results show that Al can be a chemical promoter and via engineering Al at atomic level, which is highly effective for rational design of HT-WGS catalysts with high performance.

Keywords: Water-gas shift reaction, Al promoter, Chemistry role

DOI: 10.7176/CMR/17-1-05

Publication date: March 30th 2025

1. Introduction

Due to the rapid depletion of fossil fuel, the development of clean and sustainable energy carriers has raised numerous research interests worldwide. Of them, hydrogen (H_2) is a promising alternative with high energy density and environmental friendliness, which will only emit water during combustion [1]. Conventionally, H_2 is mainly generated from catalytic steam reforming of gaseous and liquid hydrocarbon fuels (such as gasoline and natural gas), which occupies approximately 95% of the overall H_2 production. One of the disadvantages of this reforming reaction is co-generation of a huge amount of CO, which needs to be eliminated to avoid poisoning of the downstream catalysts. Currently, the removal of detrimental CO can be achieved by the following water-gas shift (WGS) reaction, which is industrially important by simultaneously transforming CO to CO_2 and producing the same quantity of H_2, as shown in Equ. (1)

$$CO+H_2O \leftrightarrow CO_2+H_2 \quad \Delta H=-41.2 \text{ kJ mol}^{-1} \quad (1)$$

Up to now, various catalysts have been prepared according to the working temperature window of WGS. In practical applications, a three-stage process is mainly implemented for WGSR: a high-temperature water gas shift (HT-WGS) reaction operated at 350-450 °C promoted by the Fe-based heterogeneous catalyst, and a low-temperature water gas shift (LT-WGS) reaction at 150-300 °C facilitated by the Cu-Zn-Al based heterogeneous catalysts. Additionally, there has been research into medium-temperature (MT-WGS) catalysts and sulfur-tolerant “sour gas” shift catalysts [2].

Herein, a series of Al doped Fe_2O_3 catalyst precursors were prepared with different Al loading amounts. Through various characterizations such as XRD, SEM and high-resolution transmission electron microscopy (HRTEM), it was suggested that the Al also worked as a chemical promoter. Particularly, the atomically dispersed Al will form $FeAl_2O_4$, which then optimizes the hydrogen-binding energy but also decreases the free energy of water formation, thus leading to excellent thermocatalytic activity of HT-WGS reaction

2. Experimental

2.1 Synthesis of Al-doped hematite catalysts.

In a typical experiment, different amounts of $FeCl_3 \cdot 6H_2O$ and $Al(NO_3)_3 \bullet 9H_2O$ was dissolved in 20 mL Milli-Q water to make the mol ratio of Al meet the requirement. Subsequently, 1 mol/L NaOH was added dropwise into the leachate until its pH reached around 4, forming a slurry that was then centrifuged at 10,000 rpm for 10 min to obtain the $Fe(OH)_3$ precipitate. The precipitate was washed three times with Milli-Q water. Afterwards, the precipitate was mixed with 40 mL of Milli-Q water and put into an ultrasonic bath for 1 h. Then 1 mol/L of NaOH solution was further dropped into the resultant slurry to adjust its final pH to 6, resulting in new slurry that was transferred into a number of 150 mL autoclaves and placed inside a preheated hot-air oven maintained at 180 °C for 24 h. Then, the autoclaves were taken out and cooled down to room temperature naturally. The obtained precipitates were filtered and immersed in ethanol for 12 h, filtered and washed with distilled water three times to remove NaOH and then with ethanol to reduce the agglomeration, and finally dried at 80 °C for 2 h.

2.2 HT-WGSR testing.

Catalytic performance was evaluated in a continuous-flow fixed bed reactor with 50-170 mg of a synthesized catalyst at 400-450 ºC under the atmospheric pressure. In each run, the catalyst was mixed with ten times the amount of pre-cleaned SiC, and then heated to 400 ºC under the protection of N_2 at a heating rate of 10 °C/min, which simultaneously removed the surface contaminants. Afterwards, the dry CO gas at a concentration of ~ 4.5 vol% was fed into the system at a flow rate of 200 ml/min for 1-2 h, until the CO_2 signal was negligible (<0.1%) in the outlet gas. Note that the dry CO gas functioned as a reducing agent for an *in-situ* reduction of Fe^{3+} into ferrous Fe^{2+}, which is expected to be the active site. After catalyst reduction, CO and steam were introduced at a concentration of ~ 4.5-5 vol% each to commission the HT-WGSR for maximum 60 min. The overall gas flow rate remained at 200 mL/min, resulting in a space velocity of 0.23-0.89 $m^3\ g_{Fe2O3}^{-1}\ h^{-1}$.

3. Results and discussion

3.1 XRD.

Fig. 1(a) shows the XRD patterns of the synthesized catalyst precursors $Fe_{2-x}Al_xO_3$. Obviously, the $Fe_{2-x}Al_xO_3$ series demonstrate a high degree of crystallinity and all the diffraction peaks are in conformity with rhombohedral α-Fe_2O_3. The doping of Al does not change the substantial crystal type of α-Fe_2O_3 (**Fig. 1(a)**). It is worth noting that, there is a slight shift of the 2θ positions of main diffraction peaks. In order to get more insights into this difference, a selected range of XRD patterns from 32 to 38 degree have been highlighted. As shown in **Fig. 1(b)**, it can be clearly seen that the 2θ positions of (1 0 4) and (1 1 0) facets show an obvious right shit as the Al content increases. According to Bragg laws: $2d\sin\theta=n\lambda$, with the same X radiation (λ=0.15406 nm), the increased 2θ value corresponds to a decrease in d-spacing, indicating the reduction of lattice parameters [3]. To investigate this, the XRD results were quantified using the software X'Pert HighScore Plus with Rietveld refinement methods and the refinement parameters and results are shown in **Table 1**. It is obvious that with the enhanced addition of Al, lattice parameters of a, c and cell volume V decrease from 5.037(89) Å, 13.768(43) Å and 302.630(3) $Å^3$ of pure α-Fe_2O_3 to 5.002(51) Å, 13.704(13) Å and 297.001(1) $Å^3$ of $Fe_{1.7}Al_{0.3}O_3$, respectively. The decrease in lattice parameters can be accounted for by noting that during the hydrothermal process, Al^{3+} entered into the α-Fe_2O_3 lattice and replaced the Fe^{3+} position, forming a stable defect-induced α-Fe_2O_3 structure, or rather, a substitutional solid solution of $Fe_{2-x}Al_xO_3$. As the ionic radius of Al^{3+} (0.053 nm) is smaller than Fe^{3+} (0.06 nm), this substitutional solid solution $Fe_{2-x}Al_xO_3$ meets the Hume-Rothery rules:

$$\%\ difference = \left|\frac{r_1 - r_2}{r_2}\right| \times 100\% \leq 15\% \quad (1)$$

Where r_1 is the solute ionic radius and r_2 is the solvent ionic radius.

Here, r_1 is for Al^{3+} and r_2 is for Fe^{3+}. The difference is 11.67% and it is smaller than 15%, favouring the formation of $Fe_{2-x}Al_xO_3$. With the increased Al addition, the isovalent substitution of Fe^{3+} by Al^{3+} would ultimately form substitutional solid solution $Fe_{2-x}Al_xO_3$, thus the parameters and cell volume of this Al-doped α-Fe_2O_3 are reduced.

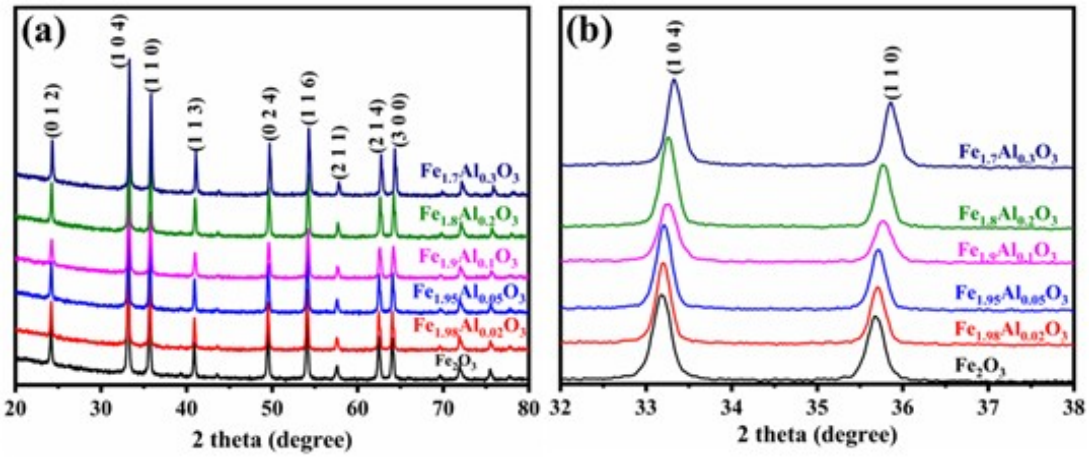

Fig. 1 XRD analysis of $Fe_{2-x}Al_xO_3$

Table 1 Lattice parameters of $Fe_{2-x}Al_xO_3$ obtained from Rietveld refinement.

Samples	Lattice parameters			Rwp/%	Good of fitness
	a/Å	c/Å	V/Å^3		
Fe_2O_3	5.037(89)	13.768(43)	302.630(3)	4.14	1.73
$Fe_{1.98}Al_{0.02}O_3$	5.036(43)	13.763(97)	302.356(9)	2.77	1.65
$Fe_{1.95}Al_{0.05}O_3$	5.025(14)	13.750(42)	300.706(6)	2.83	1.94
$Fe_{1.9}Al_{0.1}O_3$	5.020(23)	13.739(95)	299.890(7)	1.51	0.87
$Fe_{1.85}Al_{0.15}O_3$	5.010(63)	13.714(51)	298.191(7)	2.27	1.65
$Fe_{1.8}Al_{0.2}O_3$	5.006(74)	13.711(02)	297.653(1)	1.92	1.06
$Fe_{1.7}Al_{0.3}O_3$	5.002(51)	13.704(13)	297.001(1)	2.66	1.78

3.2 SEM.

Fig. 2 visualizes the $Fe_{2-x}Al_xO_3$ growth dynamic underpinning the Al variation in the hydrothermal treatment stage. For the original Fe_2O_3 without Al, the morphology shows a regular polyhedron structure with an average size of around 100 nm in diameter. After the initial addition of Al (0.34%), some tiny wrinkles appear on the surfaces of the $Fe_{1.98}Al_{0.02}O_3$ nanoparticles but the overall structure still remains consistent with the pure Fe_2O_3 sample. When the Al content was increased to 0.85%, more and more wrinkles are observed on the $Fe_{1.95}Al_{0.05}O_3$ surfaces, as shown in **Fig. 2(b)**, and it is worthy to note that the whole morphology is slightly different from the regular polyhedron shape, with some edges being replaced by some round corner. Interestingly, remarkable changes occurred when the Al content was further increased to 1.72%. As can be seen from **Fig. 2(c)**, the previous polyhedron structure is completely missing and the $Fe_{1.9}Al_{0.1}O_3$ transform into round nanoparticles, with some smaller clusters on the surfaces, which is probably due to the formation of Al-based solid solutions in hematite. The evolution of the morphology continued with the Al addition increased to higher values of 2.6%, 3.5% and 4.42%, those clusters are fully gone and the entire morphology for each single particle exhibits a round and disk-shaped morphology, as demonstrated in **Fig. 2(d-f)**. And this is due to the formation of the stable $Fe_{2-x}Al_xO_3$ solid solution, to be specific, the Fe and O reticular densities along c axis (polar facets) decline faster than those along basal facets, leading to a faster growth of the polar facets than the basal faces, which further cause a decrease of the crystal size along c axis. Therefore, the entire $Fe_{2-x}Al_xO_3$ morphology becomes thinner [4].

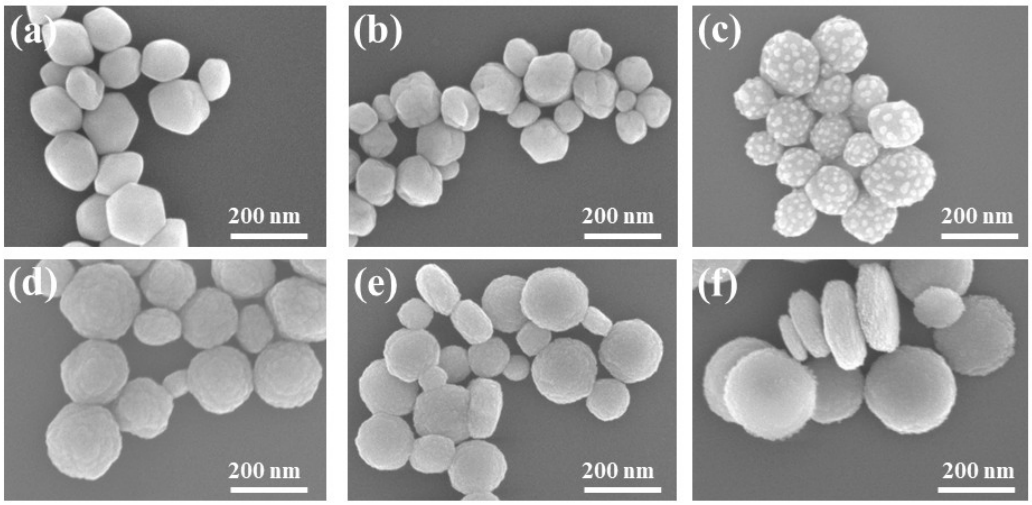

Fig. 2 SEM images of hydrothermal products for $Fe_{2-x}Al_xO_3$ (x=0.02~0.3)

3.3 HT-WGS performance-CO Conversion.

Fig. 3(a) and **(b)** display the CO conversion results of the reduced $Fe_{2-x}Al_xO_3$ catalysts at 400 and 450 °C, respectively. On the pure Fe_2O_3 catalyst, the CO conversion was comparatively low in the temperature range of interest: 3.3% and 6.8% at 400 and 450 °C, respectively. After loading of Al with an initial amount of 0.34 %, the activity was slightly improved with the CO conversion of 3.8% and 9.6% at 400 and 450 °C, respectively. Interestingly, the conversion dramatically enhanced with CO conversion of 6.3% at 400 °C and 16.2% at 450 °C, approximately 1.9 and 2.4 times than the pure Fe_2O_3 catalyst, respectively. With further increasing levels of Al content, the CO conversion is correspondingly decreased to a similar extent over $Fe_{2-x}Al_xO_3$ catalysts. For example, when the Al content was doubled (1.72%), the CO conversion showed an immediate decrease, reaching 4.5% and 13.1% at 400 and 450 °C, respectively. With further increased Al loadings, the CO conversion demonstrated constant decline of CO conversions. Surprisingly, as the Al content was increased as high as 4.42%, the CO conversion was highly similar to the pure Fe_2O_3 catalyst, namely 3.2% and 7.8% at 400 and 450 °C, respectively. In addition, the BET specific surface area of the pure hematite and the $Fe_{1.95}Al_{0.05}O_3$ catalyst are 43.62 and 44.17 m^2/g, respectively, indicating there is no structural influence of Al addition. The above result implies that low content of Al probably causes the atomic dispersion of Al atoms in the $Fe_{1.95}Al_{0.05}O_3$ catalyst. Specifically, when the Al loading level is higher than 0.85 %, some of the Al species are aggregated to form $FeAl_2O_4$ clusters, which will lose some of the active Fe^{2+}-Fe^{3+} sites during HT-WGS reaction, thus leading to the decreased CO conversion [5].

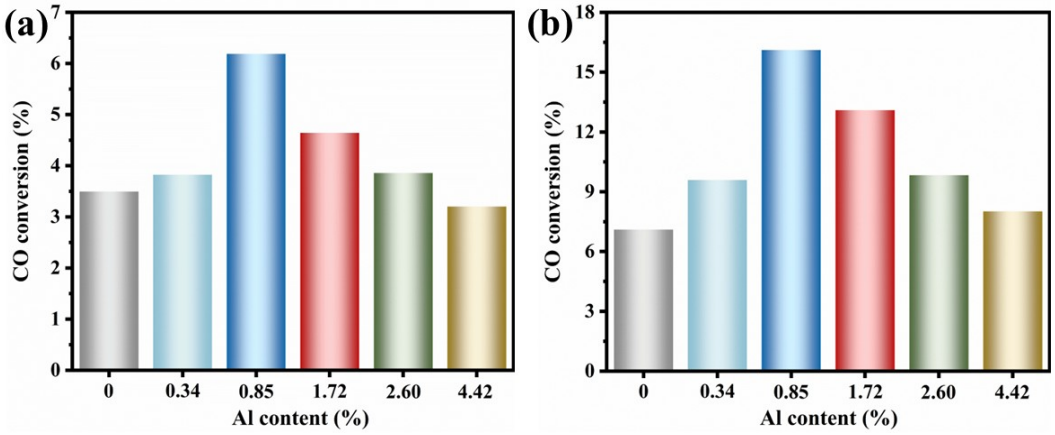

Fig. 3 (a) and (b) are stabilized CO conversion of $Fe_{2-x}Al_xO_3$ (x=0.02-0.3) at 400 and 450 ◦C, respectively.

3.4 STEM analysis (spent $Fe_{1.95}Al_{0.05}O_3$ catalyst).

Fig. 4(a) demonstrates the STEM images of the spent $Fe_{1.95}Al_{0.05}O_3$ catalyst and its corresponding selected area electron diffraction (SAED) pattern (as shown in **Fig. 4(b)**) demonstrates the presence of multiple-ring diffraction spots for the various orientations, which can be indexed to the (220), (311) and (400) facets for magnetite. It can be well observed that after the HT-WGS reaction, this catalyst still remains a similar morphology, as show in **Fig. 4(c)**. The detailed facets for this precursor are confirmed by HRTEM in **Fig. 4(d)**, demonstrating two equivalent facets of (220), and (2-2 0) with a d-spacing of 0.295 nm and are perpendicular to one each. All these feature facets belong to the [001] zone axis of magnetite [6]. Furthermore, the corresponding FFT (**Fig. 4e**) patterns indicate an inter-cross of cubic diffraction spots that can be indexed to the [001] zone axis for a single-crystal structured cubic Fe_3O_4, suggesting the spent catalyst was Fe_3O_4.

Moreover, the HAADF-STEM mapping images in **Fig. 4(f-j)** reveal that Fe and O are distributed uniformly within the magnetite matrix, which should echo the above speculation on the probable formation of solid solution that in turn prevent the overreduction of magnetite to metallic Fe. Specifically, it is worthy to note that the Al EDX mapping did not show any agglomeration, indicating that Al was atomically distributed within the catalyst. Additionally, the C mapping shows that C signal from the spent $Fe_{1.95}Al_{0.05}O_3$ catalyst was really weak, indicating that there is no carbon deposition on the catalyst surface.

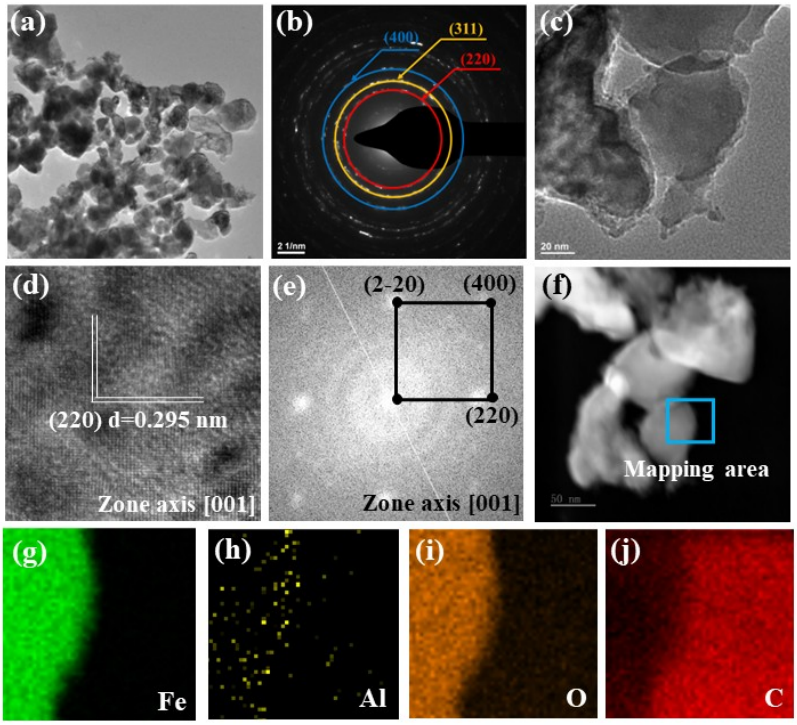

Fig. 4 STEM images of the spent $Fe_{1.95}Al_{0.05}O_3$ catalyst: (a) an overall view, (b) the corresponding SAED of (a), (c) a typical particle, (d) high-resolution TEM from (c), (e) the corresponding fast Fourier transform (FFT) image of (d), (f) HAADF-STEM image of (c), (g-j) elemental mapping of (f) with Fe (green), Al (yellow), oxygen (orange) and C (red).

4. Conclusion

In this paper, a series of $Fe_{2-x}Al_xO_3$ (x=0.02-0.3) catalyst precursors were synthesized through hydrothermal synthesis, which were subsequently reduced and then employed in the HT-WGS reaction. Through various characterizations, it can be therefore concluded that Al can also be a chemical promoter with an extremely low content of 0.85% in Fe_2O_3. Due to the additon of Al (from 0.34 to 4.42%), the spinel structured $FeAl_2O_4$ formed, which can grasb Fe^{2+} and prevent its over reduction, thus improved the CO conversion. With an extremely low amount of 0.85% Al addition, the corresponding $Fe_{1.95}Al_{0.05}O_3$ catalysts exhibited the best activity for HT-WGS

with CO conversion of 6.3% at 400 °C and 16.2% at 450 °C, approximately 1.9 and 2.4 times than the pure Fe_2O_3 catalyst. STEM confirmed that atomic isolation of Al atoms within Fe_3O_4 lattice not only optimizes the hydrogen-binding energy but also decreases the free energy of water formation, thus leading to excellent thermocatalytic activity of Al_1-Fe_2O_3 catalyst. The results show that Al can also be a chemical promoter and via engineering Al at atomic level, which will promote rational design of Fe-based HT-WGS catalysts with high performance.

Acknowledgements

The authors gratefully acknowledge the support from the Yancheng Key Research and Development Program (Social Development, YCBE202244), the Project of Education and Teaching Reform from Yancheng Teachers University (2023YCTCJGZ07) and the start-up grant (204060037) from Yancheng Teachers University.

References

[1] Zhu M, Wachs IE. Iron-Based Catalysts for the High-Temperature Water–Gas Shift (HT-WGS) Reaction: A Review. ACS Catalysis, 2016, 6: 722-732.

[2] Baraj E, Ciahotný K, Hlinčík T. The water gas shift reaction: Catalysts and reaction mechanism. Fuel, 2021, 288: 119817.

[3] Natesakhawat S, Wang X, Zhang L, Ozkan US. Development of chromium-free iron-based catalysts for high-temperature water-gas shift reaction. Journal of Molecular Catalysis A: Chemical, 2006, 260: 82-94.

[4] Li W, Y. Zuo. Mechanisms on the morphology variation of hematite crystals by Al substitution: The modification of Fe and O reticular densities. Scientific Reports, 2016, 6:35960.

[5] Yan H, Qin X, Yin Y, Teng Y, Jin Z, Jia C. Promoted Cu-Fe_3O_4 catalysts for low-temperature water gas shift reaction: Optimization of Cu content. Applied Catalysis B: Environmental, 2018, 226: 182-193.

[6] Yoo P, Liao P. Multiple redox mechanisms for water-gas shift reaction on Fe_3O_4 (111) surface: A density functional theory and mean-field microkinetic modeling study. Applied Surface Science, 2023, 630, 157501.